Cell. Mol. Life Sci. 65 (2008) 4019 – 4027
1420-682X/08/244019-9
DOI 10.1007/s00018-008-8379-5

Cellular and Molecular Life Sciences

Research Article

Zinc binding to peptide analogs of the structural zinc site in alcohol dehydrogenase: Implications for an entatic state

T. Bergman[a,b], K. Zhang[c], C. Palmberg[b], H. Jörnvall[b] and D. S. Auld[a,d,*]

[a] Center for Biochemical and Biophysical Sciences and Medicine, Harvard Medical School, Boston, MA 02115 (USA)
[b] Department of Medical Biochemistry and Biophysics, Karolinska Institutet, 171 77 Stockholm (Sweden)
[c] Department of BCPS, Illinois Institute of Technology, Chicago, IL 60616 (USA)
[d] Department of Biology, Boston College, Chestnut Hill, MA 02467 (USA), Fax: +1-617-552-2011,
e-mail: auldda@bc.edu or auld@fas.harvard.edu

Received 3 July 2008; received after revision 11 August 2008; accepted 1 September 2008
Online First 14 October 2008

Abstract. Zinc binding to the peptide replica and analogs to residues 93–115 of horse liver alcohol dehydrogenase (ADH) was examined by competition of the peptides and the chromophoric chelator 4-(2-pyridylazo)resorcinol for zinc and X-ray absorption fine structure analysis of the zinc ligands. In the enzyme, zinc is coordinated by four Cys residues. In the peptide replica, zinc is bound to three Cys and one His residue. A four-Cys zinc coordination is observed only when His is removed, leading to increased zinc stability. ADH crystal structures reveal that the ε-amino group of the conserved residue Lys323 is within H-bond distance of the backbone amide oxygens of residues 103, 105 and 108, likely stabilizing the zinc coordination in the enzyme. The peptide data thus indicate structural strain and increased energy in the zinc-binding site in the protein, characteristic of an entatic state, implying a functional nature for this zinc site.

Keywords. Zinc, alcohol dehydrogenase, synthetic peptides, 4-(2-pyridylazo)resorcinol, x-ray absorption fine structure analysis, x-ray crystallography, atomic absorption, entatic state.

Introduction

Zinc binding is important for functions and structures of many enzymes of all classes [1–3]. Medium-chain dehydrogenases/reductases (MDR enzymes) of the alcohol dehydrogenase (ADH) type are zinc metalloenzymes [4–6] with two zinc atoms per subunit, one catalytic at the active site, and the other "structural" at a site thought to affect subunit interactions [7, 8]. Like in most zinc metalloenzymes, the catalytic zinc atom interacts with three protein ligands plus a water molecule, while the structural zinc interacts with four protein ligands [8, 9].

The structural zinc site of ADH was the first to be recognized in any protein and led to the definition of structural zinc sites as consisting of one zinc bound to four protein ligands but no water [9]. Structures of over ten dozen structural zinc sites have been reported with representatives in all enzyme classes [3, 10]. While the purpose of such sites is generally thought to affect local protein conformation directly, some of these sites are now believed to influence enzyme function indirectly through the actions of the side

* Corresponding author.

chains of amino acid residues residing within the sequence between adjacent ligands (spacer arms) [10]. Efforts to classify proteins functionally have generated a pattern suggesting concurrent incorporation of both function and structure in one map that links similar functions with different structures [11]. However, the specific structural features of metal-containing enzymes suggestive of the mechanism that might account for selective reactivity and functionality are largely unknown.

Based on X-ray diffraction analysis, the structural zinc site of horse liver ADH is composed of four closely spaced Cys residues (positions 97, 100, 103, and 111 in a separate loop structure) [8, 12]. To date, function in addition to the support of a proper tertiary/quaternary structure has not been assigned to this ADH zinc site. However, early experiments suggested that the zinc ligands are susceptible to oxidation, which could lead to disulfide bridge formation [13] and, hence, loss of zinc. This type of oxidoreductive interplay between thiols/disulfides has been shown to be a general phenomenon suggested to be associated with zinc transport in metallothionein and/or metalloproteins in general [14, 15]. Results of early studies removing this zinc by dialysis were believed to establish its structural importance [6, 7, 16]. Enzymes of related type but not containing this zinc site, *e.g.*, sorbitol dehydrogenase, differ in quaternary structure [17, 18], and recombinant enzyme variants of ADH, with one each of the zinc ligands exchanged from Cys to Ala, are labile [19].

Since the ligand altered enzymes are labile, they are not ideal for the evaluation of zinc binding. We have examined peptides synthesized to correspond to the zinc binding ADH segment, with and without amino acid replacements/deletions. The peptide replica of this protein segment mimicks the metal binding stoichiometry of horse liver ADH [20]. In the present study zinc stoichiometries and metal binding affinities of replica peptide analogs are determined. The metallochromic chelator 4-(2-pyridylazo)resorcinol (PAR) is used as a competitor to extract zinc from the metal-saturated holopeptides [21]. The peptide/zinc complex is challenged with increasing concentrations of PAR, shifting the equilibrium to a $Zn(PAR)_2$ complex, which has a molar absorptivity of 61 500 $M^{-1}\,cm^{-1}$ at 500 nm (PAR absorbs at 411 nm).

Using the synthetic peptides, PAR titrations, and X-ray absorption fine structure (XAFS) analysis, we observed differences in zinc ligation that suggest that the "structural" zinc site in ADH is in a configuration that is energetically strained relative to that of the peptides, similar to that postulated for an active site of enzymes. This situation resembles that of an entatic state (derived from the Greek "entasis" (εντασις) suggesting a state that is stretched or under tension), a setting in which a group or region of an enzyme is poised for catalytic action in the absence of substrate [22–24].

Materials and methods

Peptide synthesis. Peptides and analogs were prepared from side chain protected tertiary butyloxycarbonyl amino acid derivatives using an Applied Biosystems 430A peptide synthesizer. The crude peptide preparations were obtained *via* treatment of the peptide resin with hydrogen fluoride followed by acetic acid extraction. Constituent peptides were purified by preparative reverse-phase HPLC (Vydac C_{18}) utilizing a gradient of acetonitrile in aqueous 0.1% trifluoroacetic acid. Peptide integrity was checked by amino acid analysis, mass spectrometry and Edman degradation.

Preparation of zinc peptides. HEPES buffer (20 mM, pH 7.5) was used after treatment with diphenylthiocarbazone (dithizone) to remove traces of metal ions [25]. Zinc stock solution (10 mM) was prepared in water from spectral grade zinc sulfate hepta-hydrate (Johnson Matthey Chemicals, UK). The Cys-containing peptides were reduced with a 200-fold molar excess of dithiothreitol (DTT) for 6 h at 37°C and stored at –70°C until used. DTT was removed by exclusion chromatography on a Bio-Gel P4 column (Bio-Rad). The reduced peptides were collected under anaerobic conditions within a plastic bag flushed with nitrogen, and zinc was added to fractions in a 2–10-fold molar excess. After incubation at room temperature for 5 min (pH 7.5), the excess free zinc was separated from the peptide/zinc complex *via* a second round of exclusion chromatography on Bio-Gel P4.

Zinc quantification. The zinc binding stoichiometry was evaluated by atomic absorption spectrophotometry (Perkin-Elmer 2380) and amino acid analysis (Pharmacia-LKB 4151 Alpha Plus).

Analysis of zinc coordination. The metal-ligand coordination and the average coordination distances were determined by XAFS measurements of the peptide/zinc complexes. Fractions from exclusion chromatography were concentrated about 20-fold under vacuum at room temperature in a Speedvac equipment (Savant) and used for XAFS analysis at approximately 1 mM peptide/zinc complex and about 400 mM HEPES buffer.

All XAFS measurements were performed at Beam lines X9-B and X18-B of the National Synchrotron Light Source, Brookhaven National Laboratory. The Zn K_α fluorescence, emitted after the absorption of X-ray photons, was counted by a 13-element Ge detector (Canberra), and the intensity of the incident beam was recorded by an ionization chamber filled with nitrogen gas. The incident count rate (ICR) of a single channel of the Ge detector was less than 70×10^3 s^{-1}, with a shaping time of 0.5 ms on a Canberra spectroscopic amplifier (Model 2020). The ICR was much lower than the saturation value with the detector. A series of scans were collected for each sample, and the effective counts per point totaled more than 1 million. XAFS data collected at different times with the same sample were essentially identical.

The complex $Zn(Im)_2(Ac)_2$ was chosen as the standard for the analysis of Zn-nitrogen, and Zn-oxygen coordination pairs. The Zn first shell of $Zn(Im)_2(Ac)_2$ contains two oxygen and two nitrogen atoms and is located at an average distance of 1.986 Å as determined by X-ray diffraction of the crystalline complex [26]. Since oxygen and nitrogen atoms are almost indistinguishable owing to their scattering properties, this compound is excellent for analysis of coordination shells containing both oxygen and nitrogen atoms [27]. ZnS served as the standard compound for Zn-to-S ligation. X-ray diffraction of the crystalline compound shows four sulfur atoms at 2.342 Å from the zinc ion. The two standard complexes were measured by casting their fine powder (400 mesh) on Scotch tape.

The dead time, originating from the Ge detector pulse processing electronics, was corrected to ensure the quality of the data [28]. This significantly reduces artifacts caused by beam intensity variations. The corrected experimental data were then reduced following procedures previously outlined [27, 29]. The XAFS $\chi(k)$ function was obtained by converting from energy to electron wave number k (the midpoint of the edge is taken as E_o); subtracting the pre-edge contribution with a polynomial fit and the slowly varying atomic background with a cubic spline fit; and normalization by a constant edge step. A Fourier transform was then performed with a k^2 weighting to obtain a pseudo-atomic distribution function about the absorbing atom. A single coordination shell was isolated by back transforming a desired region in the pseudo-atomic distribution function to k space. The nearest coordination shell was analyzed quantitatively by the non-linear least-squares fitting method [30] using empirical model compounds ($Zn(Im)_2(Ac)_2$ and ZnS). In these fits, we assume a nitrogen/oxygen sub-shell and a sulfur sub-shell. The fitting parameters were generally kept to $\leq$5. For a single shell, all three parameters were varied, while for two sub-shells, at least one coordination number was fixed. Error analysis of the fitting results was performed using a criterion that incorporates the degree of freedom in the data and the variation of systematic and statistical errors in k space [31]. Based on this criterion, a fit can be accepted when the quality of the fit (Q) is less or equal to unity, and rejected when larger than unity.

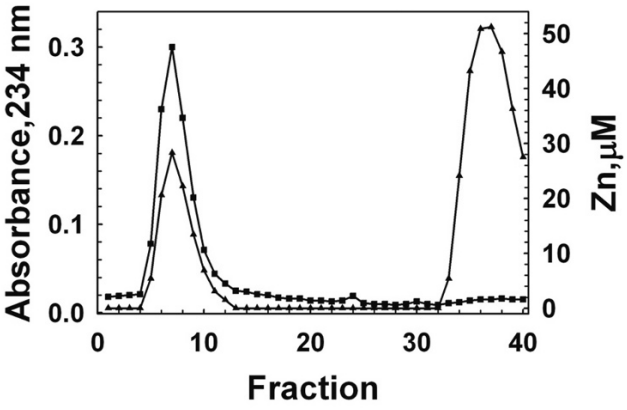

Figure 1. Exclusion chromatography of the native segment (four Cys residues, peptide 1) after incubation of the reduced peptide with zinc. Fractions were monitored at 234 nm for peptide (squares) and by atomic absorption for zinc (triangles). Formation of a peptide/zinc complex is evident and excess non-bound zinc is visible at the end of the chromatogram. Peptide structure shown in Table 1.

Stability constant determination. Titrations were carried out using a 4 mM PAR stock solution prepared from the monosodium salt hydrate (Aldrich) in 20 mM HEPES buffer, pH 7.5. For each data point, the stock solution was diluted in HEPES buffer to a suitable PAR concentration (1–1000 μM) and an aliquot of the peptide/zinc complex was added (approximately 1 μM). After mixing and waiting 3 min to ensure equilibrium, the absorbance at 500 nm was registered and corrected for background and dilution. Zinc extraction curves for the peptide analogs were generated and the equilibrium calculations were based on a PAR zinc binding constant (K_P) of 3.2×10^{11} M^{-2} and a molar absorptivity of 61 500 $M^{-1}cm^{-1}$ for the $Zn(PAR)_2$ complex, both determined *via* titration of PAR with zinc at 25°C in 20 mM HEPES, pH 7.5. An equilibrium expression combining zinc binding to both peptide (K_B) and PAR (K_P) was used in the calculations ($K_B : K_P = [peptide/Zn][PAR]^2 : [Zn(PAR)_2][peptide]$). Absorbance and spectra were measured at 25°C with a Varian Cary 1E spectrophotometer employing 1-cm-pathlength cuvettes.

Table 1. Structures, zinc-to-peptide stoichiometries, and zinc binding constants for the peptide analogs studied. The top peptide is the replica of the zinc binding alcohol dehydrogenase (ADH) segment (residues 93–115 with Cys ligands underlined), all other analogs contain specific amino acid replacements or (bottom case) deletions.

	Peptide	Zinc/peptide[a] (n = 3–10)	K_B zinc (M^{-1})[a] (n = 2–5)
	Four cysteines (replica peptide)		
1	FTPQ C GK C RV C KHPEGNF C LKND	1.1	7.0×10^{9}
	Three cysteines		
2	FTPQ A GK C RV C KHPEGNF C LKND	1.2	2.7×10^{9}
3	FTPQ C GK A RV C KHPEGNF C LKND	1.2	2.6×10^{9}
4	FTPQ C GK C RV A KHPEGNF C LKND	1.2	6.9×10^{9}
5	FTPQ C GK C RV C KHPEGNF A LKND	1.1	1.1×10^{10}
	Two cysteines		
6	FTPQ A GK A RV C KHPEGNF C LKND	1.2	6.1×10^{8}
7	FTPQ C GK A RV A KHPEGNF C LKND	1.0	7.9×10^{7}
8	FTPQ C GK C RV A KHPEGNF A LKND	0.3	7.6×10^{7}
9	FTPQ A GK C RV A KHPEGNF C LKND	0.9	1.5×10^{8}
10	FTPQ C GK A RV C KHPEGNF A LKND	0.9	7.0×10^{7}
11	FTPQ A GK C RV C KHPEGNF A LKND	0.8	8.1×10^{7}
	One cysteine		
12	FTPQ C GK A RV A KHPEGNF A LKND	0.0	–
13	FTPQ A GK C RV A KHPEGNF A LKND	0.0	–
14	FTPQ A GK A RV C KHPEGNF A LKND	0.5	3.6×10^{6}
15	FTPQ A GK A RV A KHPEGNF C LKND	0.0	–
	Zero cysteine		
16	FTPQ A GK A RV A KHPEGNF A LKND	0.0	–
	Zero histidine		
17	FTPQ C GK C RV C KAPEGNF C LKND	0.9	1.3×10^{10}
18	FTPQ C GK C RV C K —— GNF C LKND	1.0	1.5×10^{10}

[a] Arithmetic mean based on n separate experiments. The maximum variation for zinc-to-peptide stoichiometries is 13 %, and that for zinc binding constants is 20 %.

Results

A set of 18 peptides that corresponds to the loop surrounding the structural zinc atom of horse liver ADH was synthesized and tested for zinc binding. It includes the 23-residue replica and analogs of that protein segment (residues 93–115, Table 1).

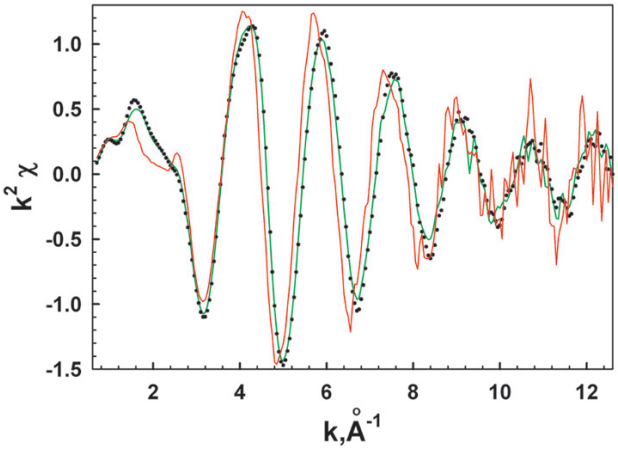

Figure 2. Zn K-edge X-ray absorption fine structure (XAFS) data for zinc peptides. Peptide 1 (green), peptide 4 (circles), and peptide 17 (red) at 150 K. Data weighted with a k^2 factor.

Zinc binding and stoichiometry. The peptides were reduced with DTT to ensure availability of Cys ligands. The DTT was then removed by exclusion chromatography under anaerobic conditions. Zinc was added at a 2–10-fold molar excess and zinc binding was measured after exclusion chromatography (Fig. 1). Zinc is bound to all peptides that contain two or more Cys ligands. The analogs containing only one Cys do not reveal detectable zinc binding, except for the peptide with a one-residue spacer to a His, corresponding to His105 of the protein (Table 1). The control (peptide 16) with Ala residues at all Cys positions gave no evidence of zinc binding.

For almost all of the peptides that bind zinc, the stoichiometries are close to 1:1 for the zinc/peptide ratio (Table 1). The exceptions are one of the analogs with two Cys (peptide 8, Table 1) and the zinc binding analog with only one Cys (peptide 14). Their stoichiometries are close to 1:2 for the zinc/peptide ratio, a fact compatible with peptide dimerization to maintain tetra-coordination of zinc bound to four Cys or two Cys/two His ligands, respectively, or to other combinations of chelating residues in peptides 8 and 14 (not evaluated in this study).

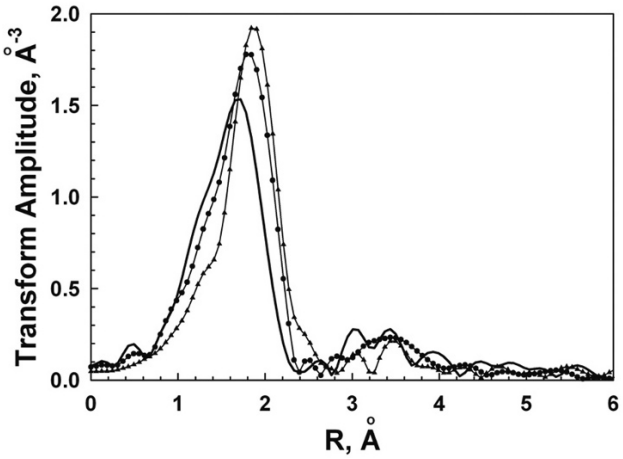

Figure 3. Fourier transforms of the XAFS χ(k) data for peptide 1 (circles), peptide 17 (triangles), and peptide 7 (solid). The k^2 χ Fourier transform was performed from 0.8 to 12.0 Å in k space using a Hanning window function.

Determination of ligands to zinc. We used XAFS to investigate the ligands to the zinc in the peptides because it can differentiate between sulfur and nitrogen/oxygen ligands very readily [32, 33]. The spectra of the weighted XAFS function, k^2 χ(k), for the peptide replica of the protein segment (peptide 1, Table 1) and that containing an Ala in place of Cys103 (peptide 4) are almost identical (Fig. 2), while they differ markedly from that of the peptide containing Ala in place of His105 (peptide 17, Fig. 2). The Fourier transforms of peptides 1 and 17, and of the peptide containing Ala in place of Cys at positions 100 and 103 (peptide 7), exhibit shifts in the peak locations and amplitudes (Fig. 3). Thus, peptides 1 and 17 have a higher apparent average interatomic distance than peptide 7. This is consistent with a zinc coordination sphere in peptide 7 that contains fewer sulfur and more nitrogen or oxygen ligands in its first shell than peptides 1 and 17. Both peptides 1 and 7 (containing His) have a peak/double peak in the Fourier transform located between 2.8 and 4.0 Å, while that for peptide 17 (His replaced by Ala) is smaller (Fig. 3). Such alterations in this region of the XAFS spectrum are characteristic of an imidazole ligand to zinc [32]. For a His residue, contribution is mainly by the 4 (5)-carbon and ε-N of the imidazole ring that is enhanced about threefold owing to a focusing effect. The presence of peaks in this particular region of the Fourier transforms for both peptides 1 and 7 (Fig. 3) therefore suggests a His residue to be involved in zinc binding of these peptides.

Least-squares fitting of the XAFS data for the first coordination shells of the zinc peptides results in 2–10 $Å^{-1}$ in k space with eight degrees of freedom [33]. Several two-shell models involving nitrogen/oxygen and sulfur binding were employed to fit the first shell data and the results are summarized in Table 2 together with the quality of fit value, Q [31]. The broad first coordination shell distribution in the Fourier transform for peptide 1 suggests the presence of O or N ligands (Fig. 3). Fitting the XAFS data for peptide 1 with a zinc coordination site containing one nitrogen/oxygen ligand at 2.03 Å and three sulfur ligands at 2.32 Å is essentially equivalent to the XAFS function for the first shell (Fig. 4), and a Q value of 0.3 (Table 2) supports this as a suitable model for zinc binding in peptide 1. In contrast, assuming an all zinc-sulfur ligand site for peptide 1 results in a best fit of 4.8 S located at 2.32 Å from the zinc atom and a Q value of 4 (Table 2). These data together with the first shell fit shown in Figure 4 suggests rejection of a four-Cys zinc coordination site in peptide 1.

Table 2. First coordination sphere fitting based on X-ray absorption fine structure (XAFS) measurements of peptide/zinc complexes. N is the zinc coordination number; R the average absorber-scatterer bond length; σ the mean square deviation in the absorber-scatterer bond length; and Q is the fitting criterion with asterisk indicating an unacceptable fit (see Table 1 for peptide numbers).

Peptide	Ligand	N	R (Å)	σ ($Å^2$)	Q
1	S	3.0	2.32	−0.001	0.3
	N/O	1.0	2.03	0.001	
	S	4.8	2.32	−0.003	4*
2	S	3.0	2.31	−0.001	1.3
	N/O	1.0	2.03	0.005	
3	S	3.0	2.33	−0.001	0.8
	N/O	1.0	2.02	0.002	
4	S	3.0	2.32	−0.001	0.3
	N/O	1.0	2.04	0.000	
5	S	2.8	2.32	−0.001	0.6
	N/O	1.3	2.03	0.002	
7	S	2.0	2.29	0.000	0.5
	N/O	1.9	2.03	0.001	
	S	3.0	2.30	0.003	2.6*
	N/O	1.0	2.03	−0.002	
	S	1.0	2.29	−0.007	2.1*
	N/O	3.0	2.02	0.007	
17	S	4.0	2.34	0.001	0.6
	S	3.0	2.33	−0.003	1.8*
	N/O	1.0	1.99	0.03	

The results for peptides 2–5 resemble those of peptide 1 (Table 2). The best fit is obtained for a zinc site containing three sulfur ligands at 2.32±0.01 Å and one

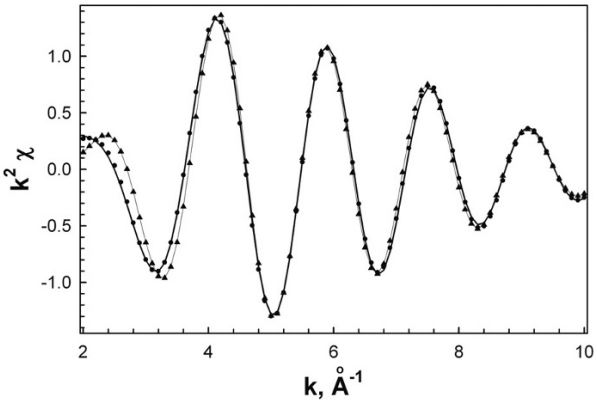

Figure 4. The first shell $k^2\chi$ function for peptide 1 (solid black line) compared with a least-squares fit of a zinc binding site containing four sulfur ligands (triangles and gray line) and a fit with one N/O ligand and three S ligands (circles).

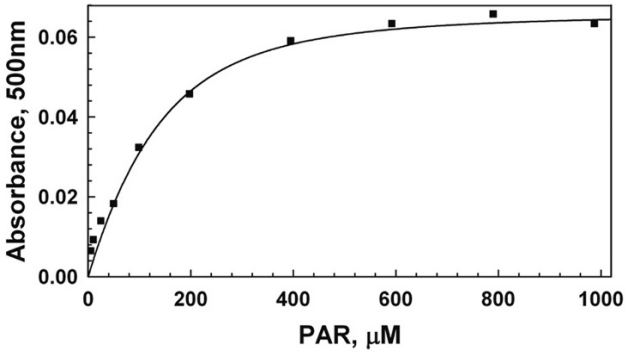

Figure 5. 4-(2-Pyridylazo)resorcinol (PAR) titration of a peptide/zinc complex with three Cys residues. Set of data for peptide 4 with theoretical line based on the average zinc binding constant 6.9×10^9 M^{-1} (Table 1). Peptide structure shown in Table 1.

N/O ligand at 2.03±0.01 Å. The XAFS function for peptide 17 can be fitted to a zinc site that contains four sulfur atoms at an average distance of 2.34 Å from the zinc atom. The inclusion of one N/O ligand renders the fit unacceptable (Table 2), suggesting that acidic residues do not participate in zinc binding of peptide 17. On the other hand, the best fit for the XAFS function for peptide 7 contains two sulfur and two N/O ligands at a fit quality of 0.5 (Table 2). This would seem to indicate the involvement of an acidic residue in addition to the imidazole. In contrast, assuming zinc coordination by one N/O and three S zinc ligands, or one S and three N/O zinc ligands increase Q to 2.6 and 2.1, respectively, rendering such sites unacceptable in peptide 7.

Thus, the data presented in Table 2 support a zinc binding model that favors a three-Cys/one-His coordination site (peptides 1–5). When His is not available (peptide 17), a four-Cys coordination site is preferred, and when the number of Cys residues is reduced to two (peptide 7), a second N/O ligand, most likely one of the acidic residues, is involved in zinc coordination.

Determination of zinc binding constants. A protocol involving competition of the peptide/zinc complex with the metallochromic chelator PAR in titrations monitored at 500 nm was employed [21]. When the PAR concentration is sufficiently high, all zinc bound to the peptide is extracted and the absorbance at 500 nm becomes constant. For the zinc bound to the peptide replica (peptide 1), a PAR concentration 1000-fold higher than that of the peptide is required, resulting in a value for the zinc binding constant of 7.0×10^9 M^{-1} (Table 1). The titration curves for the series of analogs that vary in the number of Cys residues from four to one have the same general hyperbolic shape but the corresponding zinc stabilities differ (Table 1). Going from four Cys residues in peptides 1, 17 and 18, to three in peptides 2–5, and two in peptides 6–11, the zinc stabilities decrease by three orders of magnitude (10^{10} to 10^7 M^{-1}, Fig. 5 and Table 1). Among the peptides that bind zinc, peptide 14 (with a single Cys and His) yields the lowest binding constant, decreased further by one order of magnitude to 10^6 (Table 1). For analogs containing four Cys but no His (peptides 17 and 18), tight zinc binding at the 10^{10} M^{-1} level is observed (Table 1). Theoretical plots based on average zinc binding constants calculated from values in the middle portion of the PAR titration curves are consistent with the experimental plots (Fig. 5).

Analysis of the short/long spacer motif. We also examined the influence of differently sized spacers in peptides with three potential zinc ligands (Cys/His/Cys), the short/long spacer motif observed for catalytic zinc sites [3, 34]. The His-Cys spacer is held constant at 5 residues, while the Cys-His spacer is made to vary: 1, 4 and 7 residues (peptides 6, 9 and 7). The zinc binding affinity decreases as the size of this spacer increases (Table 3).

Discussion

Liver ADH is a homodimeric enzyme containing different sets of zinc atoms localized in different regions of each subunit: one at the active site bound to Cys, His and water, the other at a "structural" site formed by four Cys residues in a separate loop. The existence and structure of this loop with four Cys ligands to zinc was considered to be an opportunity for investigation of the chemistry of a zinc atom at a protein site thought to be enzymatically inactive.

Table 3. Zinc binding constants for model peptides with two spacers, one variable (V) and one constant (C), between potential chelating residues: Cys-V-His-C-Cys. A shorter V spacer promotes tight zinc binding.

V	C	K_B (zinc, M^{-1})
7	5	7.9×10^7
4	5	1.5×10^8
1	5	6.1×10^8

The peptides are 7, 9 and 6, respectively (see Table 1).

Interestingly, the coordination pattern of the supposedly inactive structural zinc atom when analyzed in the peptide model shows that zinc is bound to three Cys and one His residue with a stability constant lower than that for a four-Cys coordination. This apparent difference to the zinc coordination in the protein [12] was not expected and therefore explored further.

For this purpose, we quantified zinc binding in a set of peptides related to the structure in the vicinity of the supposedly inactive zinc atom of liver ADH, where the number and nature of potential zinc ligands was varied systematically. The results indicate that both the number of Cys residues, the presence of His, and the spacing between Cys/His residues are important variables (Table 1). PAR proves to be effective in direct titration of peptide/zinc complexes and allows the determination of zinc binding constants. Addition of PAR to the metal-saturated peptide instead of apopeptide to the $Zn(PAR)_2$ complex, avoids problems from thiol oxidation during titration. The peptide/zinc complexes are very stable, without evidence of oxidation after days at 4°C or hours at room temperature, and binding curves of repeated PAR titrations are reproducible. Depending on the number and position of ligands, the zinc binding constants range in an ordered fashion from tight to low binding (from 10^{10} to 10^6 M^{-1}). Thus, the binding constants determined by competition with PAR reflect the nature of zinc coordination sites.

Exclusion chromatography reveals that all combinations of four, three and two Cys residues generate significant zinc binding (Table 1). However, XAFS analysis indicates that the single His residue, corresponding to His105, is a zinc ligand (Table 2, Fig. 3). The presence of His in the peptides results in a three-Cys/one-His coordination, rather than that of four Cys reported for the protein [12]. When Ala replaces His, zinc is still bound, and XAFS analysis now reveals a distinct four-Cys coordination. Regarding analogs with two Cys residues, one (peptide 7) binds zinc in a pattern that involves two S (from Cys97 and Cys111) and two N/O (one N from His105, and one O likely from Glu107 or Asp115) as ligands (Table 2).

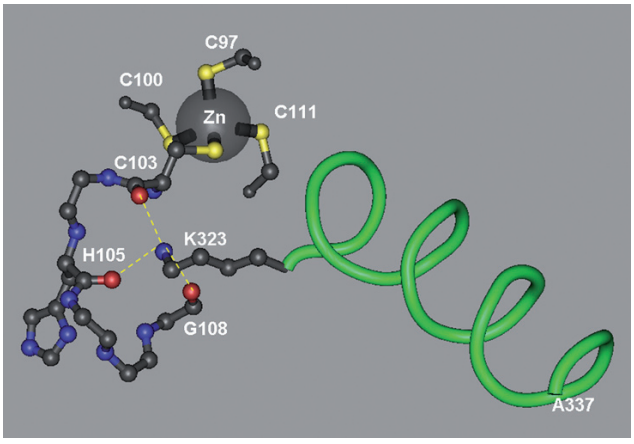

Figure 6. Three-dimensional structure of the structural zinc site of alcohol dehydrogenase (PDB# 1BTO). The helix ending with Ala337 positions the ε-amino group of Lys323 within H-bonding distance of the backbone carbonyls of amino acid residues Cys103, His105 and Gly108. Figure prepared using the program Cn3D of the National Center for Biotechnology Information.

The three-Cys/one-His coordination for the peptide replica leaves one Cys that does not bind. Judging from the zinc stability constants of the three Cys analogs (Table 1), Cys103 is a likely candidate. Peptide 4, where this Cys residue is replaced by Ala, exhibits almost the same zinc stability as the replica (peptide 1), while peptides 2, 3 and 5 all exhibit different affinities for zinc. Moreover, the XAFS spectra for the peptide replica and peptide 4, where Ala replaces Cys103, are essentially identical (Fig. 2). This further substantiates that replacement of His105 with Ala in peptide 17 results in firm zinc binding (of the order 10^{10} M^{-1}, Table 1) to the four Cys residues as observed in the XAFS analysis.

For two of the present peptide analogs, less than unity zinc-to-peptide ratios were found. Of the four analogs containing one Cys and one His residue, only one (peptide 14) reveals significant zinc binding, but at 0.5 zinc per peptide molecule (Table 1). A similar zinc-to-peptide ratio indicative of peptide dimerization was found for one of the analogs containing two Cys residues (peptide 8).

The coordination of His105 to the zinc in the peptides suggests that its replacement by Cys103 as ligand in the protein is likely accompanied by structural strain with higher energy, and which could be due to forces exerted upon Cys103 and/or residue 105 in the protein. Analysis of ADH family member sequences and three-dimensional structures provides insight into how this zinc coordination might occur and what its function might be. Alignment of 52 ADH protein sequences encompassing six classes of ADH enzymes (I, II, III, IV, V/VI, VII [35]) and their isoforms from a wide range of phyla reveals that position 105 is not

conserved and that Asn (62 %), Ser (21 %) and His (10 %) are the three residues most frequently found at that position [36]. Three-dimensional structures of ADH enzymes exist for the three major variations of residue 105. Thus, horse class I ADH (PDB# 1BTO) has His105, human class I α ADH (PDB# 1HSO) has Asn105, and mouse class II ADH (PDB# 1E3E) has Ser105. The structures show that Cys103 is directed towards the interior of the protein to ligate the zinc while the side chain of the residue at position 105 is directed to the exterior solvent with its potential zinc binding nitrogen or oxygen of the side chain 11.5–13 Å from the structural zinc atom. Further examination suggests why the residue at position 105 likely exists in this conformation. An α-helix of 14 residues extending from amino acid 324 to 337 places the ε-amino group of Lys323 within H-bonding distance of the amide carbonyl oxygens of residues 103, 105 and 108 (Fig. 6). Thus, for horse class I ADH (1BTO) the distance values are Cys103 (2.69 Å), His105 (2.64 Å) and Gly108 (2.70 Å). For human class I α ADH (1HSO) the distances are Cys103 (2.95 Å), Asn105 (2.67 Å) and Ser108 (2.70 Å), and for mouse class II ADH (1E3E) they are Cys103 (2.94 Å), Ser105 (2.96 Å) and Thr108 (2.97 Å). While the residues at positions 105 and 108 are not conserved, the interaction of their amide carbonyl oxygen with the ε-amino group of Lys323 is maintained throughout the structures. This interaction directs the side chain of residue 105 to the exterior solvent. Lys323 is conserved in all 52 sequences of the ADH enzymes, further indicating the importance of this interaction.

We can only speculate about the basis for such differences in zinc coordination of the enzyme compared with those of the peptides. Residue 105 in combination with other amino acids on the surface of the protein could potentially participate in protein complexes. A more direct involvement of the zinc site would be the modification of the Cys sulfur atoms. Examination of zinc finger structures led to the postulate that H-bonds between neighboring amides and thiolate ligands electronically stabilize the thiolates [37, 38]. Further studies of model complexes have shown that a single hydrogen bond reduces the reactivity toward an electrophile by up to two orders of magnitude [39]. These results suggest that the zinc thiolates in the ADH structural site should be unreactive towards electrophiles since there are 2–4 amide N-H bonds within 3.1–3.6 Å of each of the zinc-bound thiolates. In contrast to the deactivating effect of neighboring amide N-H on zinc thiolates, the presence of Lys and Arg side chains within 6.5 Å of Cys residues has been postulated to increase the nucleophilicity of thiolate groups [40]. This type of mechanism would require that a Cys ligand would be released from the zinc. In the protein, Cys97 might be a candidate since this residue is near the exterior solvent. The equivalent position in *E. coli* threonine dehydrogenase has been implicated in the formation of an air-dependent disulfide bond without loss of enzymatic activity [41]. In addition, the ε-amino group of Lys113 is 4.43 Å from Cys97 in the horse enzyme. In conclusion, the data show that the coordination of zinc in the peptide replica and analogs differs from that in the enzyme, suggesting that the ADH structural zinc site is in a strained conformation, typical of an entatic state [22–24]. This calls for examination of suitable derivatives to characterize a possible function.

Acknowledgement. We would like to express our sincere gratitude to Professor Bert L. Vallee, Harvard Medical School, the originator of the entatic state concept, for his generous support and interest in the project. This work was supported by grants from the Swedish Research Council (03X-3532, 03X-10832, 629-2002-8654, 621-2003-3616, 621-2005-5377), the Swedish Cancer Society (4159), the Endowment for Research in Human Biology, Inc., NIH Grant GM-47534 (DSA and KZ), the Knut and Alice Wallenberg Foundation, the Emil and Wera Cornell Foundation and the Swedish Society of Medicine.

1 Vallee, B. L. and Auld, D. S. (1990) Zinc coordination, function, and structure of zinc enzymes and other proteins. Biochemistry 29, 5647–5659.
2 Auld, D. S. (2001) Zinc coordination sphere in biochemical zinc sites. Biometals 14, 271–313.
3 Auld, D. S. (2005) Zinc enzymes. In: Encyclopedia of Inorganic Chemistry, vol. IX, pp. 5885–5927, King R. B. (ed.), John Wiley & Sons, Chichester.
4 Vallee, B. L. and Hoch, F. L. (1957) Zinc in horse liver alcohol dehydrogenase. J. Biol. Chem. 225, 185–195.
5 Åkeson, Å. (1964) On the zinc content of horse liver alcohol dehydrogenase. Biochem. Biophys. Res. Commun. 17, 211–214.
6 Drum, D. E., Li, T. K. and Vallee, B. L. (1969) Considerations in evaluating the zinc content of horse liver alcohol dehydrogenase preparations. Biochemistry 8, 3783–3791.
7 Sytkowski, A. J. and Vallee, B. L. (1976) Chemical reactivities of catalytic and noncatalytic zinc or cobalt atoms of horse liver alcohol dehydrogenase: differentiation by their thermodynamic and kinetic properties. Proc. Natl. Acad. Sci. USA 73, 344–348.
8 Brändén, C.-I., Jörnvall, H., Eklund, H. and Furugren, B. (1975) Alcohol dehydrogenase. In: The Enzymes, vol. 11, pp. 103–190, Boyer P. D. (ed.), Academic Press, New York.
9 Vallee, B. L. and Auld, D. S. (1990) Active-site zinc ligands and activated H_2O of zinc enzymes. Proc. Natl. Acad. Sci. USA 87, 220–224.
10 Auld, D. S. (2004) Structural zinc sites. In: The Handbook of Metalloproteins, vol. 3, pp. 403–415, Messerschmidt, A., Bode, W. and Cygler, M. (eds.), John Wiley & Sons, Chichester.
11 Vendruscolo, M. and Dobson, C. M. (2005) A glimpse at the organization of the protein universe. Proc. Natl. Acad. Sci. USA 102, 5641–5642.
12 Eklund, H., Nordström, B., Zeppezauer, E., Söderlund, G., Ohlsson, I., Boiwe, T., Söderberg, B.-O., Tapia, O., Brändén, C.-I. and Åkeson, Å. (1976) Three-dimensional structure of horse liver alcohol dehydrogenase at 2.4 Å resolution. J. Mol. Biol. 102, 27–59.

13 Jörnvall, H. (1973) Differences in thiol groups and multiple forms of rat liver alcohol dehydrogenase. Biochem. Biophys. Res. Commun. 53, 1096–1101.
14 Maret, W. and Vallee, B. L. (1998) Thiolate ligands in metallothionein confer redox activity on zinc clusters. Proc. Natl. Acad. Sci. USA 95, 3478–3482.
15 Maret, W. (2004) Zinc and sulfur: A critical biological partnership. Biochemistry 43, 3301–3309.
16 Formicka-Kozlowska, G., Schneider-Bernlöhr, H., von Wartburg, J.-P. and Zeppezauer, M. (1988) $H_8Zn(c)_2$ and $Zn(c)_2$ $Co(n)_2$ human liver alcohol dehydrogenase. Eur. J. Biochem. 173, 281–285.
17 Jeffery, J., Chesters, J., Mills, C., Sadler, P. J. and Jörnvall, H. (1984) Sorbitol dehydrogenase is a zinc enzyme. EMBO J. 3, 357–360.
18 Jörnvall, H., von Bahr-Lindström, H. and Jeffery, J. (1984) Extensive variations and basic features in the alcohol dehydrogenase-sorbitol dehydrogenase family. Eur. J. Biochem. 140, 17–23.
19 Jeloková, J., Karlsson, C., Estonius, M., Jörnvall, H. and Höög, J.-O. (1994) Features of structural zinc in mammalian alcohol dehydrogenase. Site-directed mutagenesis of the zinc ligands. Eur. J. Biochem. 225, 1015–1019.
20 Bergman, T., Jörnvall, H., Holmquist, B. and Vallee, B. L. (1992) A synthetic peptide encompassing the binding site of the second zinc atom (the 'structural' zinc) of alcohol dehydrogenase. Eur. J. Biochem. 205, 467–470.
21 Bergman, T., Palmberg, C., Jörnvall, H., Auld, D. S. and Vallee, B. L. (1999) Zinc binding characteristics of the synthetic peptide corresponding to the structural zinc site of horse liver alcohol dehydrogenase. Adv. Exp. Med. Biol. 463, 339–342.
22 Vallee, B. L. and Williams, R. J. P. (1968) Metalloenzymes: The entatic nature of their active sites. Proc. Natl. Acad. Sci. USA 59, 498–505.
23 Williams, R. J. P. (1995) Energised (entatic) states of groups and of secondary structures in proteins and metalloproteins. Eur. J. Biochem. 234, 363–381.
24 Behnke, W. D. and Vallee, B. L. (1972) The spectrum of cobalt bovine procarboxypeptidase A, an index of catalytic function. Proc. Natl. Acad. Sci. USA 69, 2442–2445.
25 Holmquist, B. (1988) Elimination of adventitious metals. Methods Enzymol. 158, 6–12.
26 Horrocks, W. D., Ishley, J. N. and Whittle, R. R. (1982) Models for Cobalt(II)-substituted zinc metalloenzymes. 1. Comparison of the crystal structures of complexes of the type $[M(RCOO)_2(Im)_2]$ (Im = Imidazole; M = Co, Zn; R= CH_3, C_2H_5). Inorg. Chem. 21, 3265–3269.
27 Zhang, K., Chance, B., Auld, D. S., Larsen, K. S. and Vallee, B. L. (1992) X-ray absorption fine structure study of the active site of zinc and cobalt carboxypeptidase A in their solution and crystalline forms. Biochemistry 31, 1159–1168.
28 Zhang, K., Rosenbaum, G. and Bunker, G. (1993) The correction of the dead time loss of the Ge detector in x-ray absorption spectroscopy. Jpn J. Appl. Phys. 32 Suppl. 32–2, 147–149.
29 Zhang, K. and Auld, D. S. (1993) XAFS studies of carboxypeptidase A: Detection of a structural alteration in the zinc coordination sphere coupled to the catalytically important alkaline pKa. Biochemistry 32, 13844–13851.
30 Stern, E. A. and Heald, S. M. (1983) In: Handbook of Synchrotron Radiation, vol. 1B, pp. 955–1014, Koch, E.-E., Eastman, D. E. and Farge, Y. (eds.) North-Holland, New York.
31 Zhang, K., Stern, E. A., Ellis, F., Sanders-Loehr, J. and Shiemke, A. K. (1988) The active site of hemerythrin as determined by X-ray absorption fine structure. Biochemistry 27, 7470–7479.
32 Bunker, G., Stern, E. A., Blankenship, R. E. and Parson, W. W. (1982) An x-ray absorption study of the iron site in bacterial photosynthetic reaction centers. Biophys. J. 37, 539–551.
33 Lee, P. A., Citrin, P. H., Eisenberger, P. and Kincaid, B. M. (1981) Extended x-ray absorption fine structure – Its strengths and limitations as a structural tool. Rev. Mod. Phys. 53, 769–806.
34 Vallee, B. L. and Auld, D. S. (1989) Short and long spacer sequences and other structural features of zinc binding sites in zinc enzymes. FEBS Lett. 257, 138–140.
35 Nordling, E., Persson, B. and Jörnvall, H. (2002) Differential multiplicity of MDR alcohol dehydrogenases: enzyme genes in the human genome *versus* those in organisms initially studied. Cell. Mol. Life Sci. 59, 1070–1075.
36 Protein Information Resource. www-nbrf.georgetown.edu.
37 Maynard, A. T. and Covell, D. G. (2001) Reactivity of zinc finger cores: Analysis of protein packing and electrostatic screening. J. Am. Chem. Soc. 123, 1047–1058.
38 Blake, P. R., Park, J. B., Adams, M. W. W. and Summers, M. F. (1992) Novel Observation of NH–S(Cys) hydrogen-bond-mediated scalar coupling in ^{113}Cd-substituted rubredoxin from *Pyrococcus furiosus*. J. Am. Chem. Soc. 114, 4931–4933.
39 Smith, J. N., Hoffman, J. T., Shirin, Z. and Carrano, C. J. (2005) H-bonding interactions and control of thiolate nucleophilicity and specificity in model complexes of zinc metalloproteins. Inorg. Chem. 44, 2012–2017.
40 Britto, P. J., Knipling, L. and Wolff, J. (2002) The local electrostatic environment determines cysteine reactivity of tubulin. J. Biol. Chem. 277, 29018–29027.
41 Clark-Baldwin, K., Johnson, A. R., Chen, Y.-W., Dekker, E. E. and Penner-Hahn, J. E. (1998) Structural characterization of the zinc site in *Escherichia coli* L-threonine dehydrogenase using extended X-ray absorption fine structure spectroscopy. Inorg. Chim. Acta 275–276, 215–221.